Design of Automatic Detection Algorithm for Dislocation Contrasts in Birefringence Images of SiC Wafers

Akira Kawata[1†], Kenta Murayama[2], Shogo Sumitani[1,3] and Shunta Harada[4*]

[1]*Graduate School of Informatics, Kyoto University, Yoshida-Hommachi, Sakyo-ku, Kyoto 606-8501, Japan*

[2]*Mipox Corporation, 31F, Shinjuku Nomura Building,1-26-2, Nishishinjuku, Shinjuku-ku Tokyo, Japan 163-0531, Japan*

[3]*Anamorphosis Networks, Yoshida-Hommachi, Sakyo-ku, Kyoto 606-8501, Japan*

[4]*Center of Integrated Research for Future Electronics (CIRFE), Institute of Materials and Systems for Sustainability (IMaSS), Nagoya University, Furo-cho, Chikusa-ku, Nagoya, 464-8601, Japan*

*Corresponding author's e-mail: shunta.harada@nagoya-u.jp

†Now at Preferred Networks Inc.

Birefringence imaging is one of the powerful methods for nondestructive characterization of defects in the semiconductor crystals. However, due to the complicated and unclear contrasts of dislocations in the birefringence image, it was considered to be difficult to automatically detect the position of the dislocation contrasts by the conventional image processing. In the present study, we designed the automatic detection algorithm for the dislocation contrasts taking into account for the characteristic feature of the dislocation contrasts, which were always pair of black and white contrasts. To detect the large change in the contrast level near the dislocation contrast, the automatic detection algorithm was constructed by using variance filter. Finally, we succeeded in detecting the position of the dislocation contrasts with relatively high precision and sensitivity.

1. Introduction

Crystalline defects in semiconductor devices, especially in power devices, adversely affect the performance, the reliability and the yield of the devices[1–4]. In the case of silicon (Si), a method for manufacturing a dislocation-free wafer has been established[5]. However, a lot of dislocations exists in the other power device materials such as silicon carbide (SiC), gallium nitride (GaN) and diamond compared to Si[6–8]. Therefore, it is important to detect the dislocations in the wafers. Especially, the demand for the dislocation inspection of SiC wafers have been increasing since the SiC power devices have already started to be applied to practical used.

Dislocations in SiC crystals have been detected by X-ray topography and molten KOH etching[9–12]. Photoluminescence imaging has often used for the observation in SiC epitaxial layers and semi-insulating SiC wafers[1,13–15]. For the inspection of dislocations in n-type SiC wafers for the power device application, birefringence imaging using a polarized light microscope is a promising method[16]. The contrast in the birefringence image originates from the strain field in the crystal. Therefore, it is possible to detect a dislocation from the birefringence contrast by the strain field accommodating with the dislocation. The birefringence imaging has advantage in the measurement time as well as the detailed analysis for the characteristic of dislocations. Not only the Burgers vector but also the line vector of the dislocation is possibly deduced from the dislocation contrasts caused by the different strain field. Since Bond and Andrus reported the observation of stress field accommodating with edge dislocations in silicon, defects in various kinds of crystals were detected[17–22]. As for the defects in SiC, micropipe-induced birefringence were intensively studied both experimental observation and theoretical image simulation[23–25]. Dislocations in SiC wafer were reported to observed from the comparison of synchrotron x-ray topography measurements[25,26]. However, because of the complicated and unclear contrast of the dislocations in birefringence image, and the contrast modulation due to the macroscopic stress field, it is sometimes difficult to recognize the dislocation contrast and almost impossible to automatically detect the positions of the dislocations by the conventional image thresholding[27]. In the present study, firstly, we investigated the characteristic of the dislocation contrast by comparing the birefringence image with the synchrotron X-ray topography image at the same wafer positions. Then, we designed an image processing for

the automatic detection of the dislocation contrasts, considering the characteristic of the dislocation contrasts. Finally, we proposed an algorithm to detect the position of the dislocation contrasts in birefringence image using variance filter[28]. In this article, we show not only the result of the automatic detection but also the designing process for the automatic detection algorithm.

2. Experimental methods

Two kinds of SiC crystals were used for the birefringence imaging. One is a semi-insulating (SI) 4H-SiC wafer with 4 degrees off-cut toward [11-20] grown by chemical vapor deposition. Both sides of the wafer were planarized by the chemical-mechanical polishing (CMP) and the thickness of the wafer is 150 μm. The other is a commercial n-type 4H-SiC wafer with 4 degrees off-cut toward [11-20] grown by physical vapor transport method. The Si face of the wafer was planarized by CMP and the C face was planarized by mechanical polishing, and the thickness of the wafer is 350 μm. The birefringence imaging was conducted by using an XS-1 microscope (Mipox), which is a crossed-Nicols-type transmission microscope with parallel irradiation light to observe the retardation of light passing through specimens. The detail of the configuration was shown in Ref. 22. The images are digitally recorded with the pixel resolution of about 1.8 μm/pixel.

For the comparison, synchrotron x-ray topography images were taken at the same position as the birefringence image. Grazing incident reflection synchrotron topography using monochromatic x-ray beam with 8.27 keV was conducted in BL8S2 in Aichi synchrotron radiation center, Japan. The applied g vector was 11-28. The topography image was recorded on the nuclear emulsion plates (Ilford) and digitally recorded by the optical microscope with the transmission illumination.

3. Results and discussion

3.1 Birefringence observation

Figure 1 shows the comparison between the birefringence image and the x-ray topography image of the SI 4H-SiC wafer with both side CMP. In the x-ray topography image as shown in Fig. 1(b), threading edge dislocations (TEDs) are imaged as small circular contrasts and threading screw dislocations (TSDs) are imaged as large circular contrasts. At the positions

of the threading dislocations, contrasts were always observed in the birefringence image. It seems that the contrasts patterns are depending on the Burgers vector of the dislocations. Detailed analysis of the contrast variation depending on the Burgers vector will be published elsewhere. Of importance to note that the contrasts of the threading dislocations were always the pair of black and white contrasts. The origin of such contrast of dislocations in birefringence image is related to the fact that the threading dislocation always accommodates with both compressive and tensile stress field[22]. As shown in Fig. 1, the dislocations in the SI wafer with both CMP can be clearly observed. On the other hand, the commercial SiC wafer is of n-type and the backside is usually not finished with CMP.

Figure 2 shows the birefringence image taken from the n-type 4H-SiC wafer (CMP/MP). Different from the image shown in Fig. 1, some dislocation contrasts were linear shapes, which indicates that the threading dislocations were tilted from the observation direction[26,29]. The contrast level of the image was more unclear than that of the SI wafer, which is considered to be due to the diffuse scattering on the back side with MP and the optical absorption of the n-type wafer. Furthermore, the contrast modulation by the macroscopic strain field was observed (the lower left of Fig. 2 is darker than the other area). Therefore, it is almost impossible to identify the position of the dislocation by the conventional image processing such as thresholding. However, we can recognize the position of the dislocation contrast by human eyes, because the dislocation contrasts are also always the pair of black and white contrast. Here, we focused on this characteristic feature of the dislocation contrasts for the detection of the automatic detection.

3.2 Automatic detection algorithm

Considering the characteristic feature of the dislocation contrasts, the variance filter was selected in order to detect the large local change in the contrast level. The variance filter was sometimes used for the edge detection of the photographic images[30]. One can easily imagine that filters which calculate the gradient or the similar value of the contrast level, such as the Laplacian filter and the Sobel filter, are also good choice for the automatic detection.

Figure 3 shows the flow chart of the present algorithm for the detection of the dislocation contrasts. Firstly, the 8-bit birefringence image was linearly normalized so that the averaged pixel values of a normalized image became 128 (the center of the dynamic

range) and the variance of pixel values became certain value (v_0). The normalization process makes it possible to detect the dislocation contrasts with good reproducibility even for the images having different contrast levels. Then, a variance filter was applied to the normalized image. The variance filter algorithm consists of replacing a central pixel values with the variance of a square set of n by n (n is an odd number) pixels values surrounding it. The values of the variance are large at the position where the contrast level is changing. Therefore, the values of the variance are expected to be large near the dislocation contrasts. After that, we binarized the image using a user-defined threshold value (x_0) and get a black and white image. In this image, a white pixel means that the corresponding variance value is larger than the threshold value. Then, we labeled white pixels so that each group of connecting white pixels has the same label. Finally, we calculated the minimum rectangle for each group, eliminated the smaller size of rectangles than a threshold value (S_0).

3.3 Results of the automatic detection

Figure 4 shows the results of the variance filter, the thresholding and the automatic detection for the birefringence image of the n-type 4H-SiC wafer shown in Fig. 2. A set of the tuned parameters used for the automatic detection is summarized in Table I. The variance of the position near the dislocation contrast is large and the contrast modulation in the background hardly noticed in the variance mapping shown in Fig. 4(a). After the thresholding, small particle-like contrasts due to the noise of the detector appeared at the position where the dislocation contrast is absent (Fig. 4(b)). However, owing to the area thresholding for a size of rectangles, the small particle-like contrasts were hardly surrounded by rectangles in Fig. 4(c). Finally, almost all dislocation contrasts were found to be detected by the current algorithm with relatively high accuracy.

If you closely look at the results of the automatic detection, you will find two types of erroneous detection. One type is that multiple dislocation contrasts are counted as one dislocation contrast (the largest rectangle located at upper right in Fig. 4(c)). Here, we call a “multiple-detection (MD)” error. Another type is that the very weak contrasts were not detected (true negative: TN), which was observed above the largest rectangle in Fig. 4(c). Of course, these errors can be avoided by changing a set of parameters. However, changing the parameters evoke the other errors. If you increase the values of x_0, you can eliminate the

MD errors, but TNs will increase. If you decrease the values of x_0, you can eliminate TNs, but the position where there is no dislocation contrast will be wrongly detected (false positive: FP). The set of the parameters used in the current automatic detection was tuned so as to avoid an occurrence of FPs. Therefore, occurrences of these two types of erroneous detections is considered to indicate a limitation of this detection algorithm. Table II summarizes the results of the automatic detection for 5 different images. Most of the dislocation contrasts were correctly detected (true positive: TP) and the precision (TP / (TP + FP)) were 100% because we can set the parameters so as to avoid the occurrence of FPs. The sensitivity (TP / (TP + FN)) and MD error rate (MD / TP) were 95%±2.9% and 4%±2.7%, respectively. Note that the error of the sensitivity and MD error rate was evaluated by the 95% confidence interval. The result of the automatic detection for the birefringence image was comparable to that for the etch pit counting of semiconductor wafers[31,32].

The present results indicate that threading dislocation density and the position of commercial SiC wafers are possible to be detected by the birefringence imaging as well as the current automatic detection algorithm using variance filter. This implies that the birefringence imaging is the candidate for a non-destructive inspection method for the threading dislocations in SiC wafers. Non-destructive inspection of SiC wafers is considered to contribute the efficient production of SiC power device and the improvement of the crystal quality for SiC wafers.

4. Conclusions

Automatic detection algorithm for the dislocation contrasts of n-type SiC wafers in a birefringence image was designed taking into account for the characteristic feature of the dislocation contrasts. To detect the large change in the contrast level near the dislocation contrast, the automatic detection algorithm was constructed by using variance filter. Finally, we succeeded in detecting the position of the dislocation contrasts with relatively high precision and sensitivity. The present results indicate that the birefringence imaging is one of the dislocation inspection methods for SiC wafers and will contribute the development of SiC power devices as well as the improvement of the crystal quality of SiC wafers.

Acknowledgments

The authors gratefully acknowledge Mr. Mizutani and Mr. Nakagawa (Mipox Co. Ltd) for the support of this study.

References

1) T. Kimoto, Jpn. J. Appl. Phys. **54**, 040103 (2015).

2) S. Fujita, Jpn. J. Appl. Phys. **54**, 030101 (2015).

3) S. Ohmagari, H. Yamada, N. Tsubouchi, H. Umezawa, A. Chayahara, S. Tanaka, and Y. Mokuno, Appl. Phys. Lett. **113**, 032108 (2018).

4) S. Usami, Y. Ando, A. Tanaka, K. Nagamatsu, M. Deki, M. Kushimoto, S. Nitta, Y. Honda, H. Amano, Y. Sugawara, Y.Z. Yao, and Y. Ishikawa, Appl. Phys. Lett. **112**, 182106 (2018).

5) W.C. Dash, J. Appl. Phys. **30**, 459 (1959).

6) T. Kimoto, Prog. Cryst. Growth Charact. Mater. **62**, 329 (2016).

7) Y. Zhang, A. Dadgar, and T. Palacios, J. Phys. D. Appl. Phys. **51**, 273001 (2018).

8) S. Shikata, Diam. Relat. Mater. **65**, 168 (2016).

9) M. Dudley, X.R. Huang, and W.M. Vetter, J. Phys. D. Appl. Phys. **36**, 30 (2003).

10) T. Ohno, H. Yamaguchi, S. Kuroda, K. Kojima, T. Suzuki, and K. Arai, J. Cryst. Growth **260**, 209 (2004).

11) M. Katsuno, N. Ohtani, J. Takahashi, H. Yashiro, and M. Kanaya, Jpn. J. Appl. Phys. **38**, 4661 (1999).

12) Y. Yao, Y. Ishikawa, Y. Sugawara, H. Saitoh, K. Danno, H. Suzuki, Y. Kawai, and N. Shibata, Jpn. J. Appl. Phys. **50**, 075502 (2011).

13) M. Tajima, E. Higashi, T. Hayashi, H. Kinoshita, and H. Shiomi, Appl. Phys. Lett. **86**, 1 (2005).

14) M. Tajima, E. Higashi, T. Hayashi, H. Kinoshita, and H. Shiomi, Mater. Sci. Forum **527**–**529**, 711 (2006).

15) G. Feng, J. Suda, and T. Kimoto, J. Appl. Phys. **110**, 033525 (2011).

16) B.K. Tanner and D.J. Fathers, Philos. Mag. **29**, 1081 (1974).

17) W.L. Bond and J. Andrus, Phys. Rev. **101**, 1211 (1956).

18) R. Bullough, Phys. Rev. **110**, 620 (1958).

19) K. Maiwa, K. Tsukamoto, I. Sunagawa, C. Ge, and N. Ming, J. Cryst. Growth **98**, 590 (1989).

20) N. Ming and C. Ge, J. Cryst. Growth **99**, 1309 (1990).

21) L. Hoa, T. Ouisse, D. Chaussende, M. Naamoun, A. Tallaire, and J. Achard, Cryst.

Growth Des. **14**, 5761 (2014).
22) A. Tanaka, S. Inotsume, S. Harada, K. Hanada, Y. Honda, T. Ujihara, and H. Amano, Phys. Status Solidi **257**, 1900553 (2020).
23) T. Ouisse, D. Chaussende, and L. Auvray, J. Appl. Crystallogr. **43**, 122 (2010).
24) X. Ma, M. Parker, and T.S. Sudarshan, Appl. Phys. Lett. **80**, 3298 (2002).
25) X. Ma and T. Sudarshan, J. Electron. Mater. **33**, 450 (2004).
26) T. Ouisse, D. Chaussende, and L. Auvray, J. Appl. Crystallogr. **43**, 122 (2010).
27) L. Hoa, T. Ouisse, and D. Chaussende, J. Cryst. Growth **354**, 202 (2012).
28) A. Kawata, K. Murayama, S. Sumitani, and S. Harada, Ext. Abstr. Solid State Device Mater. 217 (2020).
29) X. Ma and T. Sudarshan, in *J. Electron. Mater.* (Springer New York LLC, 2004), pp. 450–455.
30) P.A. Wilson, Photogramm. Eng. Remote Sens. **63**, 485 (1997).
31) E. Peiner and A. Schlachetzki, J. Electron. Mater. **21**, 887 (1992).
32) G. Hahn and M. Fleck, Comput. Mater. Sci. **183**, 109886 (2020).

Figure Captions

Table I. A set of the parameters used for the automatic detection.

Table II. Results of the automatic detection for 5 different images.

Fig. 1. The birefringence image (a) and the x-ray topography image (b) of the SI 4H-SiC wafers. Black arrows indicate the positions of threading edge dislocations and a white arrow indicates the position of the threading screw dislocation.

Fig. 2. The birefringence image of the n-type 4H-SiC wafer.

Fig. 3. The flow chart of the automatic detection algorithm using the variance filter.

Fig. 4. (a) The variance mapping, (b) thresholding image and (c) result of the automatic detection of the birefringence image shown in Fig. 2. The positions of the dislocation contrasts were automatically surrounded by green rectangles.

Table I. A set of the parameters used for the automatic detection.

Parameters	Values	Descriptions
v_0	16	A value of a variance for the normalization.
n	5	A size of variance filter
x_0	24	A threshold value for the variance value
S_0	10	A threshold value for a size of rectangles

Table II. Results of the automatic detection for 5 different images.

Image #	True positive	MD error	True negative	False positive
1	32	4	0	0
2	45	2	3	0
3	13	0	1	0
4	54	0	5	0
5	46	2	1	0
Total	190	8	10	0

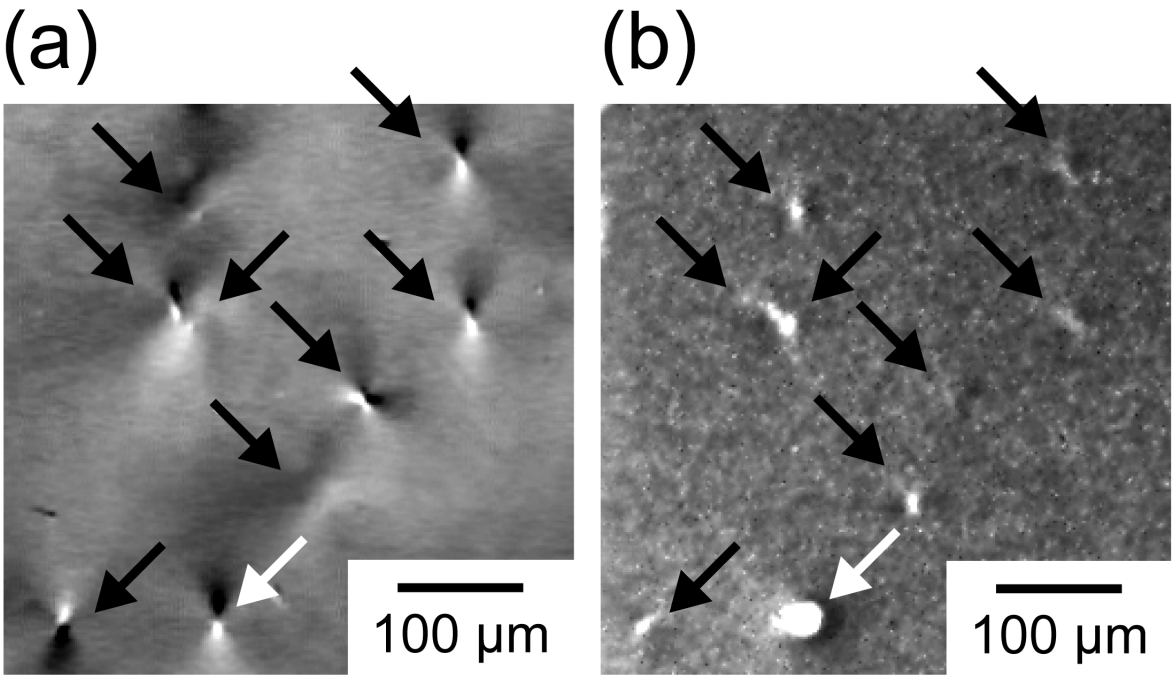

Fig. 1. The birefringence image (a) and the x-ray topography image (b) of the SI 4H-SiC wafer. Black arrows indicate the positions of threading edge dislocations and a white arrow indicates the position of the threading screw dislocation.

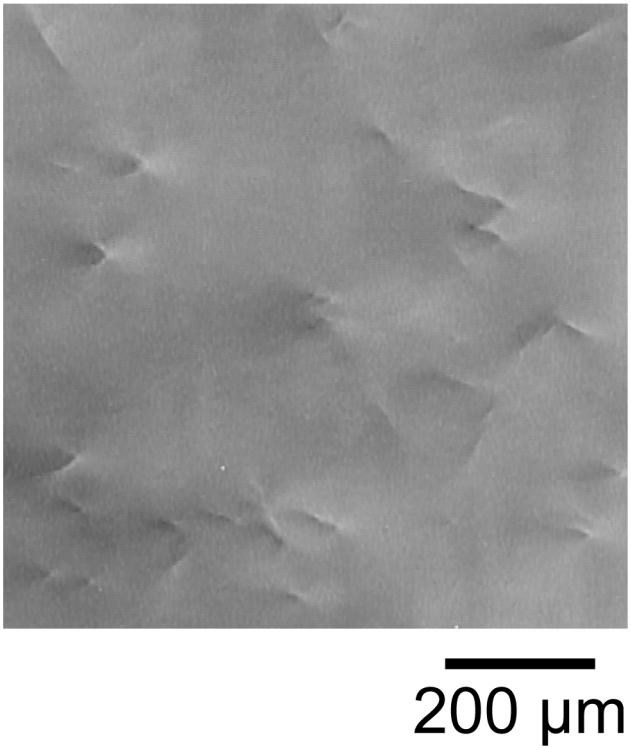

Fig. 2. The birefringence image of the n-type 4H-SiC wafer.

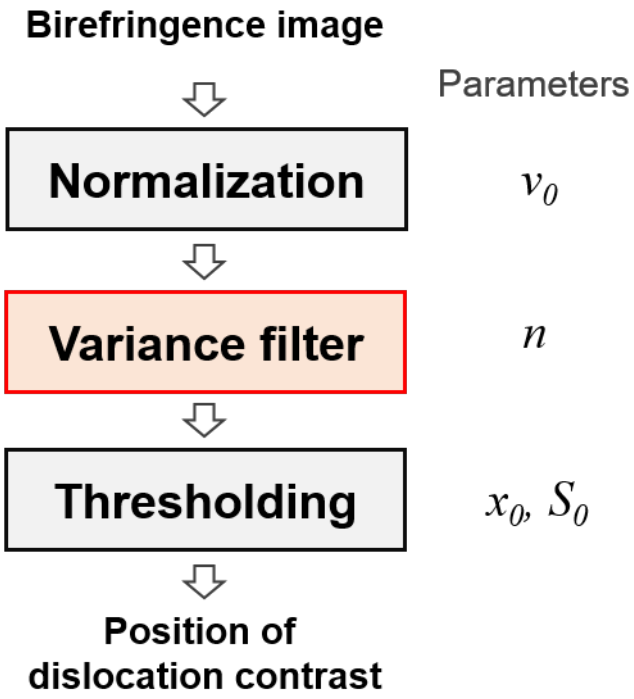

Fig. 3. The flow chart of the automatic detection algorithm using the variance filter.

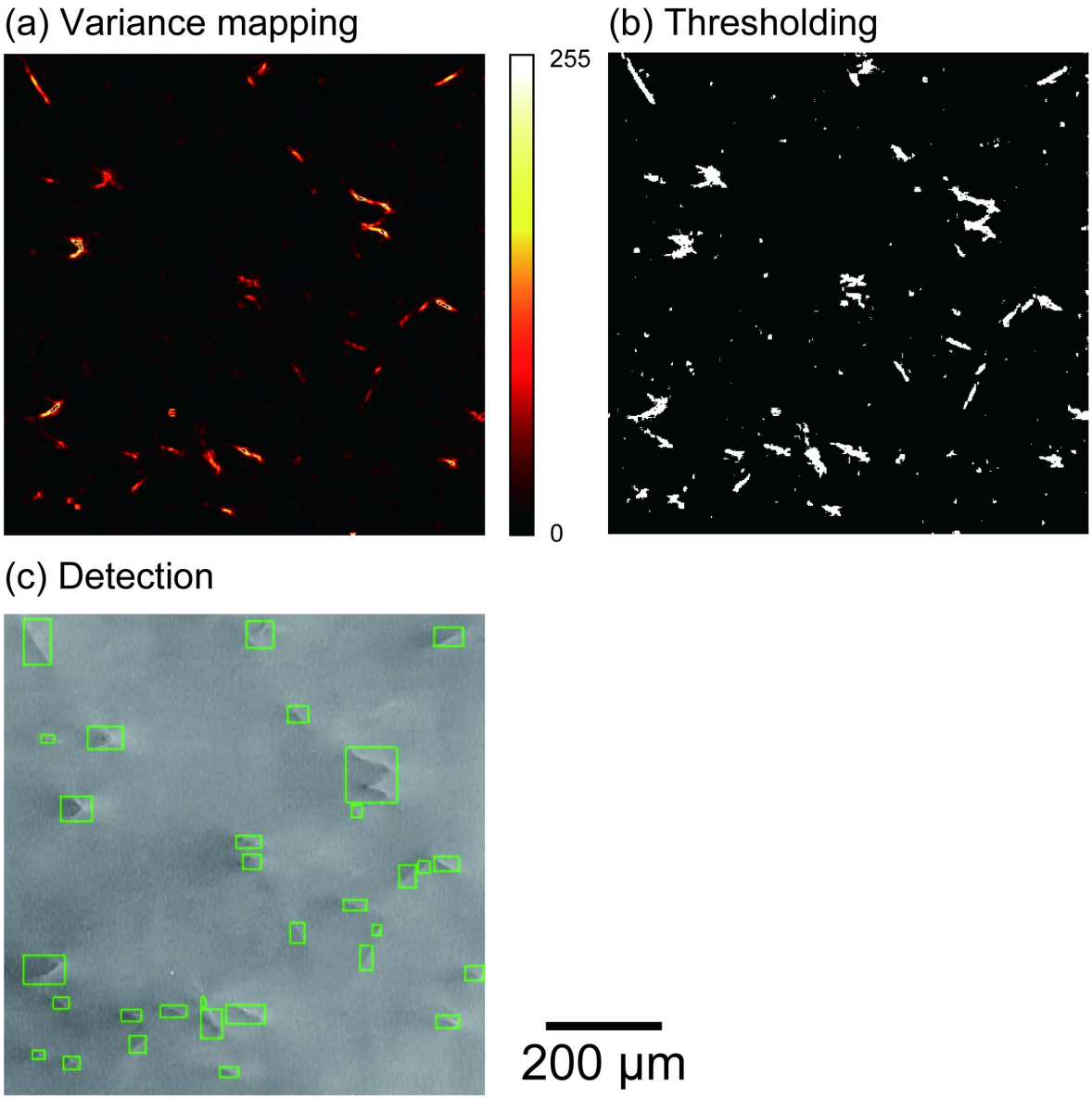

Fig. 4. (a) The variance mapping, (b) thresholding image and (c) result of the automatic detection of the birefringence image shown in Fig. 2. The positions of the dislocation contrasts were automatically surrounded by green rectangles.